

## The crystal structure of althausite, $Mg_4(PO_4)_2(OH,O)(F,\square)$

CHRISTIAN RØMMING

*Kjemisk Institutt, Universitetet i Oslo, Blindern, Oslo 3, Norway*

AND GUNNAR RAADE

*Institutt for Geologi, Universitetet i Oslo, Blindern, Oslo 3, Norway*

### Abstract

The crystal structure of althausite was solved by direct methods and refined to a final  $R$  value of 0.022 for 1164 high-angle reflections ( $\sin \theta/\lambda > 0.45 \text{ \AA}^{-1}$ ) with  $I > 2.5\sigma$ . The position of the hydrogen atom was found from a difference Fourier synthesis. The structure is orthorhombic  $Pnma$  with  $a = 8.258(2)$ ,  $b = 6.054(2)$ ,  $c = 14.383(5) \text{ \AA}$ . Magnesium atoms occur in both five- and six-fold coordination, and the coordination polyhedra are highly distorted. The Mg octahedra form chains along  $b$  by edge-sharing. Hydroxyl and fluorine occur in a largely ordered distribution among two different structural sites and occupy alternating positions along 'channels' parallel to  $b$ . Partial vacancy in the (OH,F) sites is confirmed, the population factor for the F site being 81 percent. The crystal-chemical formula of althausite is therefore  $Mg_4(PO_4)_2(OH,O)(F,\square)$  with  $Z = 4$ .

The cleavages in althausite, {001} perfect and {101} distinct, occur along planes crossing relatively few bonds and leave the chains of Mg octahedra unbroken. Bond-strength calculations for althausite and wagnerite are presented and the OH content in wagnerite is discussed.

Preliminary results of hydrothermal syntheses indicate the existence of a series from F-wagnerite to OH,F-wagnerite and from OH-althausite to OH,F-althausite. Infrared spectra of fluorine-free althausite show a splitting of the O-H stretching frequency, proving that two distinct hydroxyl positions are present.

### Introduction

The new magnesium-phosphate mineral althausite was described from serpentine-magnesite deposits in Modum, south Norway, by Raade and Tysseand (1975). Based on a wet-chemical analysis, the empirical formula was given as  $Mg_2PO_4(OH_{0.37}F_{0.25}O_{0.19}\square_{0.19})$ , with vacancy in the (OH,F) sites because of a presumed substitution of the type  $2(OH,F)^- \rightleftharpoons O^{2-}\square$ . Althausite is orthorhombic with  $a = 8.258(2)$ ,  $b = 14.383(5)$ ,  $c = 6.054(2) \text{ \AA}$ ,  $V = 719.0(7) \text{ \AA}^3$ ,  $Z = 8$ . The space group was given as  $Pna2_1$ , but from the extinctions, another possible space group is  $Pnam$  which was omitted. Furthermore, the cleavage was stated to be perfect along {001} and distinct along {101}. New investigations show that the correct cleavages are {010} (perfect, pinacoidal) and {110} (distinct, prismatic). A set of rough measurements of the angle between the face normals of the perfect and the distinct cleavage planes gave 60–63°, in good

agreement with the calculated value,  $(010) \wedge (110) = 60.14^\circ$ . The optical orientation must be changed accordingly to  $X = c$ ,  $Y = b$ ,  $Z = a$ , OAP (010), and the hardness on {010} is  $3\frac{1}{2}$  in the  $c$  direction and 4 in the  $a$  direction.

The type locality for althausite is the Tingelstadjern quarry, Modum, and the original description was based on material from this occurrence. The mineral has also been found in a similar deposit farther to the north, the Overntjern quarry. Here the althausite has a reddish-brown color and occurs in a somewhat different mineral association (talc, magnesite, brown apatite, partly enstatite). However, a more complete account of the mineral parageneses and the distribution of phosphate minerals among the deposits is reserved for a separate paper.

A microprobe analysis of the Overntjern althausite using Tingelstadjern althausite as standard gave the following result (data calculated as direct ratios after background correction; values for the Tingelstadjern

Table 1. Weight loss vs. H<sub>2</sub>O + CO<sub>2</sub> content for althausite and two apatites

	Weight loss from TGA (rel. units)	Wt% of H <sub>2</sub> O and CO <sub>2</sub> ; calculated relative units in parentheses	
Althausite	61	H <sub>2</sub> O	1.87% (60.4)
Cl-apatite	46	H <sub>2</sub> O + CO <sub>2</sub>	1.47% (47.5)
(OH,F)-apatite	41	H <sub>2</sub> O + CO <sub>2</sub>	1.27% (41.0)

material, after subtraction of apatite impurity and recalculation to 100 percent, are given in parentheses): MgO 50.5 (51.0), P<sub>2</sub>O<sub>5</sub> 44.4 (45.1), F 3.04 (2.99) weight percent. The iron content was determined with the probe using a fayalite standard: total iron as FeO is 0.40 and 0.80 weight percent in the Tingelstadjern and Overntjern althausites respectively. The higher iron content of the Overntjern mineral should be noted. Its brown color is due to microscopic inclusions of iron oxides/hydroxides.

The Overntjern occurrence has provided a few specimens with subhedral crystals of althausite imbedded in magnesite or talc. The crystals are elongated along *c* and flattened on *b*. Some natural sections  $\perp c$  show the forms {010} and {110}. One subhedral crystal has the approximate size *a*:*b*:*c* = 2:1:3 cm and shows the form {010} and four distinct terminal faces at one end of the crystal. Two of these faces belong to the same form, identified as {131}. The two other faces do not belong to the same form and no simple indices could be attached to them. These must be regarded as vicinal faces, developed because of imperfect growth of the crystal, which may be ultimately due to defects in the crystal structure, e.g. in this case partly empty (OH,F) sites (*cf.* Terpstra and Codd, 1961, p. 360–363).

The defect structure of althausite is clearly substantiated by the present structure determination, but we would still like to mention other evidence which supports the correctness of the original chemical analysis. Firstly, the new mineral holtedahlite, (Mg,Na)<sub>2</sub>(PO<sub>4</sub>,CO<sub>3</sub>,OH)(OH,F), also from the Tingelstadjern occurrence, was analyzed with the electron microprobe using althausite as standard, with H<sub>2</sub>O and CO<sub>2</sub> being determined separately with a Perkin-Elmer 240 elemental analyzer. In this way a perfectly stoichiometric formula was obtained for holtedahlite (Raade and Mladeck, 1979). Secondly, the weight losses were obtained from TGA runs on althausite and two associated apatites from Tingelstadjern. The H<sub>2</sub>O and CO<sub>2</sub> contents of the apatites were also determined with the elemental ana-

lyzer (Table 1). The internal consistency of the data is excellent (H<sub>2</sub>O value for althausite from Raade and Tysseland, 1975).

In the original description of althausite, the choice of axes was made according to the scheme  $c < a < b$ . In the structural description which follows, *b* and *c* are interchanged in order to have the space-group symbol in the standard setting, *Pnma*. The two cleavages thus become {001} and {101} in the transformed axial system.

### Experimental

The cleavage fragment used for the structure determination came from the Tingelstadjern quarry, Modum; it had approximate dimensions 0.2 × 0.2 × 0.05 mm. The X-ray diffraction data were collected on a Picker four-circle punched-card controlled diffractometer using graphite crystal monochromated MoK $\alpha$  radiation. A unique set of intensities was measured, using the  $\theta/2\theta$  scan mode with a scan rate of 2° min<sup>-1</sup> ( $2\theta$ ). The scan range was from 0.9° below  $2\theta(\alpha_1)$  to 0.9° above  $2\theta(\alpha_2)$ ; background counts were taken for 30 sec at each of the scan limits. Out of the 1631 reflections with  $\sin\theta/\lambda < 0.8\text{\AA}^{-1}$ , 1456 were regarded as observed, their intensity being larger than 2.5 times the estimated standard deviation. The variance of the intensity was taken as  $\sigma^2(I) = C_T + (0.02 C_N)^2$  where  $C_T$  is the total number of counts and  $C_N$  is the net count. Three standard reflections measured for every 100 reflections of the data set showed no systematic variations. The intensity data were corrected for Lorenz and polarization effects and for absorption [ $\mu(\text{MoK}\alpha) = 10.07 \text{ cm}^{-1}$ ].

### Structure determination

Intensity statistics gave convincing evidence of a centric structure, indicating the space group *Pnma* (after reorientation according to *International Tables for X-ray Crystallography*) rather than *Pna2*<sub>1</sub> as reported earlier (Raade and Tysseland, 1975).

The positions of all non-hydrogen atoms were found by direct methods using the program assembly MULTAN (Germain *et al.*, 1971) and refined by successive Fourier syntheses and least-squares calculations. So far the fluorine and hydroxyl oxygen atoms could not be differentiated because of the similarity in scattering power. A difference Fourier synthesis revealed the position of a hydrogen atom close to one of these atoms, however, which could thus be identified as the oxygen atom.

The composition of althausite found from chemical analysis indicates that the hydroxyl and fluorine positions are partially occupied and in part replaced

Table 2. Atomic coordinates and thermal parameters for althausite

Atom	X	Y	Z	U11	U22	U33	U12	U13	U23
Mg(1)	0.13402(5)	0.00414(7)	0.16858(3)	0.0067(2)	0.0049(2)	0.0085(2)	0.0009(1)	0.0004(1)	0.0009(1)
Mg(2)	0.34763(7)	0.25	0.42143(4)	0.0054(2)	0.0066(3)	0.0111(3)	0.0	0.0021(2)	0.0
Mg(3)	0.07712(7)	0.25	0.57505(4)	0.0068(2)	0.0063(2)	0.0075(2)	0.0	-0.0007(2)	0.0
P(1)	0.48845(5)	0.25	0.14583(3)	0.0037(2)	0.0041(2)	0.0048(2)	0.0	-0.0001(1)	0.0
P(2)	0.22456(5)	0.25	0.84820(3)	0.0043(2)	0.0045(2)	0.0055(2)	0.0	0.0004(1)	0.0
O(11)	0.38234(10)	0.04123(15)	0.14137(6)	0.0061(3)	0.0069(3)	0.0112(3)	-0.0013(3)	0.0006(2)	-0.0006(3)
O(12)	0.60739(15)	0.25	0.06273(9)	0.0064(4)	0.0112(5)	0.0072(4)	0.0	0.0012(3)	0.0
O(13)	0.59147(16)	0.25	0.23554(8)	0.0102(5)	0.0080(5)	0.0065(4)	0.0	-0.0029(3)	0.0016(3)
O(21)	0.11583(10)	0.04268(15)	0.85336(6)	0.0068(3)	0.0071(3)	0.0120(3)	-0.0016(3)	-0.0004(2)	0.0
O(22)	0.32077(16)	0.25	0.75588(8)	0.0108(5)	0.0076(5)	0.0076(4)	0.0	0.0035(4)	0.0
O(23)	0.34092(15)	0.25	0.93021(9)	0.0068(4)	0.0187(6)	0.0085(4)	0.0	-0.0028(4)	0.0
F	0.33500(15)	0.25	0.56627(8)	0.0064(7)	0.0066(7)	0.0057(7)	0.0	-0.0016(3)	0.0
O	0.09124(15)	0.25	0.07585(8)	0.0060(4)	0.0082(5)	0.0071(4)	0.0	0.0008(3)	0.0
H	0.154(7)	0.25	0.035(4)	B=1.6(7)					

The values of X, Y, Z are given in fractional coordinates, the anisotropic temperature factor is of the form  $\exp(-2\pi^2(U_{11} a^2 + U_{22} b^2 + U_{33} c^2 + 2U_{12} a b + 2U_{13} a c + 2U_{23} b c))$ . Estimated standard deviations in parentheses refer to the last digits.

by oxygen ions. The further refinement by full-matrix least-squares methods included positional parameters, anisotropic thermal parameters (for all atoms except for the hydrogen atom which was refined isotropically), and occupancy factors for hydroxyl and fluorine. Atomic scattering factors used were those of Doyle and Turner (1968) for P, Mg and O, of *International Tables for X-ray Crystallography* (1962) for F<sup>-</sup>, and of Stewart *et al.* (1965) for hydrogen. In order to reduce systematic errors due to faulty assessment of atomic charge in the atomic form factors, only diffraction data with  $\sin\theta/\lambda > 0.45\text{\AA}^{-1}$  were applied for the last stage of refinement, reducing the number of applied observations to 1164.

No significant shift occurred in the hydroxyl occupancy factor; it was consequently fixed at its normal value for a fully occupied site. The fluorine site population factor converged to 81(1) percent of the corresponding value.

The refinements converged to a conventional *R* factor of 0.022 for the reflections employed in the refinements (*R* = 0.025 for all observed reflections), *R*<sub>w</sub> = 0.031, and *S* =  $[\sum w\Delta F^2/(m - n)]^{1/2} = 1.76$ . The overdetermination ratio was 16.2.

The quantity minimized in the least-squares calculations was  $\sum w\Delta F^2$ , where *w* is the inverse of the variance of the observed structure factor. A description of the computer programs applied is given by Groth (1973).

A rigid-body analysis showed that the thermal motion of the phosphate ions to a good approximation could be interpreted in terms of translational and librational oscillation. The bond lengths used in the discussion of these ions are those corrected for libration.

A difference Fourier map had its largest electron density at (0.442, 0.250, 0.560), 0.94Å from the fluorine site. The integrated peak amounted to about 1/4 of an electron, and, although indicative of the replacement of some OH<sup>-</sup> for the F<sup>-</sup> ion, it was not included as a partially occupied hydrogen atomic position in the refinement, even if the presence of such an atom is probably significant.

The final atomic positional and thermal parameters are listed in Table 2. Interatomic distances and bond angles are reported in Table 3; estimated standard deviations are calculated from the variance-covariance matrix and include uncertainties in cell dimensions. Observed and calculated structure factors with estimated standard deviations are on deposit at the Business Office of the Mineralogical Society of America.<sup>1</sup>

<sup>1</sup> To obtain a copy of this table, order Document AM-80-133 from the Mineralogical Society of America, Business Office, 2000 Florida Avenue, N.W., Washington, D. C. 20009. Please remit \$1.00 in advance for the microfiche.

Table 3. Interatomic distances (Å) and angles (°) for althausite (with estimated standard deviations in parentheses)

Mg(1)-O(11)	2.100(1)		0(11)-Mg(1)-O	88.22(4)	0	-Mg(1)-O(13)	83.08(4)				
Mg(1)-O	2.031(1)		0(11)-Mg(1)-F	80.36(4)	F	-Mg(1)-O(21)	85.26(4)				
Mg(1)-F	2.145(1)		0(11)-Mg(1)-O(21)	160.58(4)	F	-Mg(1)-O(22)	81.80(4)				
Mg(1)-O(21)	2.107(1)		0(11)-Mg(1)-O(22)	90.97(5)	F	-Mg(1)-O(13)	176.89(5)				
Mg(1)-O(22)	2.022(1)		0(11)-Mg(1)-O(13)	102.35(5)	0(21)	-Mg(1)-O(22)	99.87(5)				
Mg(1)-O(13)	2.060(1)		0	-Mg(1)-F	95.55(4)	0(21)	-Mg(1)-O(13)	91.75(5)			
			0	-Mg(1)-O(21)	80.21(4)	0(22)	-Mg(1)-O(13)	99.59(5)			
			0	-Mg(1)-O(22)	177.33(4)						
Mg(2)-F	2.086(2)		F	-Mg(2)-O(12)	80.58(5)	0(12)	-Mg(2)-O	172.33(6)			
Mg(2)-O(12)	1.997(1)		F	-Mg(2)-O(21)	119.00(3)	0(21)	-Mg(2)-O(21)	119.97(6)			
Mg(2)-O(21)	2.048(1)		F	-Mg(2)-O	91.75(5)	0(21)	-Mg(2)-O	82.07(3)			
Mg(2)-O	2.012(1)		0(12)	-Mg(2)-O(21)	101.59(3)						
Mg(3)-F	2.133(1)		F	-Mg(3)-O(11)	82.15(3)	0(11)	-Mg(3)-O(23)	100.53(3)			
Mg(3)-O(11)	2.034(1)		F	-Mg(3)-O(23)	174.38(6)	0(11)	-Mg(3)-O(12)	116.41(3)			
Mg(3)-O(23)	1.952(1)		F	-Mg(3)-O(12)	79.42(5)	0(23)	-Mg(3)-O(12)	94.97(3)			
Mg(3)-O(12)	1.998(2)		0(11)	-Mg(3)-O(11)	120.38(6)						
0	-Mg(1)	2.031(1)	Mg(1)-O	-Mg(1)	94.39(6)	0	-H	-O(23)	176(5)		
0	-H	0.78(6)	Mg(1)-O	-H	112(2)	0	-O(23)-P(2)		96.29(7)		
0	-Mg(2)	2.012(1)	Mg(1)-O	-Mg(2)	99.28(5)	H	-O(23)-P(2)		95(2)		
0	-O(23)	2.939(2)	H	-O	-Mg(2)	133(4)					
F	-Mg(1)	2.145(1)	Mg(1)-F	-Mg(1)	91.74(5)	Mg(3)-F	-Mg(2)		96.26(5)		
F	-Mg(3)	2.133(1)	Mg(1)-F	-Mg(3)	94.50(4)						
F	-Mg(2)	2.086(2)	Mg(1)-F	-Mg(2)	132.78(3)						
			corr.								
P(1)	-O(11)	1.540(1)	1.543	0(11)-P(1)	-O(12)	109.22(4)	0(11)	-P(1)	-O(11)	110.43(7)	
P(1)	-O(12)	1.547(1)	1.550	0(11)	-P(1)	-O(13)	110.36(4)				
P(1)	-O(13)	1.545(1)	1.549	0(12)	-P(1)	-O(13)	107.19(7)				
P(2)	-O(21)	1.546(1)	1.549	0(21)	-P(2)	-O(22)	109.84(4)	0(21)	-P(2)	-O(21)	108.70(7)
P(2)	-O(22)	1.547(1)	1.551	0(21)	-P(2)	-O(23)	109.25(4)				
P(2)	-O(23)	1.522(1)	1.526	0(22)	-P(2)	-O(23)	109.94(8)				
Mg(1)-O(11)-Mg(3)	98.94(4)		Mg(1)-O(11)-P(1)	129.48(5)		Mg(3)-O(11)-P(1)	129.68(5)				
Mg(2)-O(12)-Mg(3)	103.74(6)		Mg(2)-O(12)-P(1)	122.86(8)		Mg(3)-O(12)-P(1)	133.39(8)				
Mg(1)-O(13)-Mg(1)	92.62(6)		Mg(1)-O(13)-P(1)	130.75(4)							
Mg(1)-O(21)-Mg(2)	94.70(4)		Mg(1)-O(21)-P(2)	132.16(6)		Mg(2)-O(21)-P(2)	129.87(6)				
Mg(1)-O(22)-Mg(1)	99.22(6)		Mg(1)-O(22)-P(2)	128.89(3)							
Mg(3)-O(23)-H	137(1)		Mg(3)-O(23)-P(2)	126.94(8)		H	-O(23)-P(2)		95(1)		

### Description of the structure

A stereoscopic view of the structure is presented in Figure 1; the numbering of the atoms may be seen from Figures 2, 3, and 4.

There are three non-equivalent Mg<sup>2+</sup> ions of which one is situated in a general eight-fold position [Mg(1)] and two are located on mirror planes [Mg(2) and Mg(3)]. Two non-equivalent phosphate ions have the phosphorus and two of the oxygen atoms on

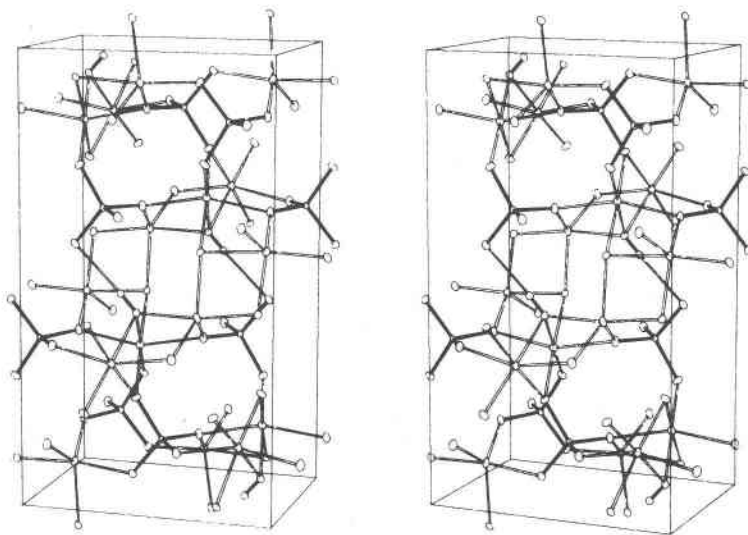


Fig. 1. Stereoscopic pair of the althausite structure. One unit cell is shown ( $b < a < c$ ); some additional atoms outside the unit cell have been included in order to complete the Mg and P polyhedra. Phosphate groups and OH groups are indicated by filled bonds. Fig. 2 (together with Figs. 3 and 4) can be used as a legend for identifying the different atomic positions.

mirror planes and two equivalent oxygen atoms in general positions. The hydroxyl and fluorine ions are situated on mirror planes.

Mg(1) (in general position) is coordinated in a distorted octahedron to one fluorine, one hydroxyl, and four phosphate oxygen atoms. The coordinations of the two other magnesium ions are distorted trigonal bipyramidal, Mg(2) with ligands  $F^-$ ,  $OH^-$  and three phosphate oxygen atoms and Mg(3) with ligands  $F^-$  and four phosphate oxygen atoms. The arrangements are visualized in Figure 3, which also shows the way in which the polyhedra are connected. Each Mg(1) octahedron shares edges with two other Mg(1) octahedra, one Mg(2) and one Mg(3) trigonal bipyramid. The Mg(1) octahedra form straight chains parallel to the  $b$  axis (*cf.* Fig. 2). The Mg(2) polyhedron shares edges with two Mg(1) octahedra and one Mg(3) trigonal bipyramid; the Mg(3) polyhedron shares edges with two Mg(1) octahedra and one Mg(2) trigonal bipyramid.

The arrangements around the anions are visualized in Figure 4. The two phosphate groups form nearly ideal tetrahedra with O–P–O bond angles in the range 107.2–110.4°. Seven of the eight phosphate oxygen atoms are coordinated to two magnesium ions, the last oxygen atom O(23) being engaged in a hydrogen bond to a hydroxyl ion and an ionic bond to a Mg(3) ion. These arrangements are all close to planar, as can be seen from the angle sums around the oxygens, which vary between 354.1 and 360.0°.

The fluorine ion is coordinated to two Mg(1) ions,

one Mg(2), and one Mg(3) ion, the fluorine site being close to the center of the Mg(1)–Mg(1)′–Mg(2) triangle (Fig. 4c). The possible hydrogen position for a hydroxyl-substituted fluorine site (*cf.* Structure determination) is completing a distorted trigonal bipyramidal arrangement with the Mg(3)–H direction as the trigonal axis.

The hydroxyl ion, in addition to the hydrogen bond to a phosphate oxygen atom O(23), is coordinated to two Mg(1) ions and one Mg(2) ion in a tetrahedral arrangement.

An important feature of the structure is that the  $OH^-$  and  $F^-$  anions occupy alternating positions along the  $b$  axis, such that a kind of 'double channel' is formed by two adjacent rows of  $OH^-/F^-$  (Fig. 2). Along  $b$ , the distances F–O and F–H are 3.093 and 3.06 Å respectively, whereas across the channels the corresponding distances (between F and OH situated at the same height above the plane  $ac$ ) are a little shorter, 2.942 and 3.02 Å respectively.

## Discussion

### Relation to other structures

Althausite belongs to a group of minerals with general formula  $M_2(XO_4)_Z$ , where M is a divalent metal atom (Mg, Fe, Mn, Cu, Zn), X is P or As, and Z is mainly OH and/or F (*cf.* Richmond, 1940). Four different types of crystal structures are known among these minerals. Tarbuttite,  $Zn_2PO_4OH$ , is triclinic, space group  $P\bar{1}$ ,  $Z = 2$  (Cocco *et al.*, 1966) and is

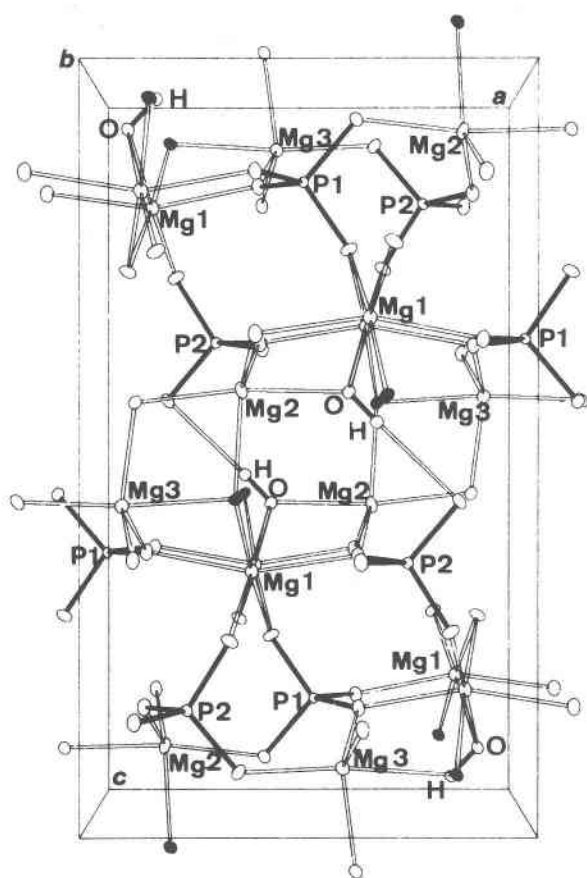


Fig. 2. The crystal structure of althausite viewed down the  $b$  axis (origin for the labelled axes is at the upper left corner of the bottom plane). The P-O and O-H bonds are filled and the F atoms are shown as filled ellipsoids. The Mg(1) octahedra form chains parallel to the  $b$  axis by edge-sharing, and the individual octahedra are only slightly separated in this projection. Note the two adjacent rows of alternating OH and F along the  $b$  axis, an arrangement that results in a sort of 'double channel' in the structure. This figure may serve as a legend to the stereoscopic views of Fig. 1.

isostructural with paradamite,  $\text{Zn}_2\text{AsO}_4\text{OH}$ . Triplite,  $(\text{Mn},\text{Fe})_2\text{PO}_4\text{F}$ , and the isostructural iron analogue zwieselite are monoclinic, space group  $I2/a$ ,  $Z = 8$  (Waldrop, 1969). The structure of these two minerals is closely related to that of wagnerite,  $\text{Mg}_2\text{PO}_4\text{F}$  (Coda *et al.*, 1967), triploidite/wolfeite,  $(\text{Mn},\text{Fe})_2\text{PO}_4\text{OH}$  (Waldrop, 1970), and sarkinite,  $\text{Mn}_2\text{AsO}_4\text{OH}$  (Dal Negro *et al.*, 1974), which form a series of monoclinic isostructural minerals with space group  $P2_1/a$  and  $Z = 16$ , *i.e.* with a doubling of the  $b$  axis in comparison with triplite/zwieselite. Another structure type is displayed by the orthorhombic minerals libethenite,  $\text{Cu}_2\text{PO}_4\text{OH}$  (Walitzi, 1963), ada-

mite,  $\text{Zn}_2\text{AsO}_4\text{OH}$  (Hawthorne, 1976; Hill, 1976), and eveite,  $\text{Mn}_2\text{AsO}_4\text{OH}$  (Moore and Smyth, 1968), which all have the space group  $Pnmm$  with  $Z = 4$ . To this series also belongs olivenite,  $\text{Cu}_2\text{AsO}_4\text{OH}$ , space group  $P2_1/n$  [with  $a$  as the unique axis and  $\alpha = 90.0(1)^\circ$ ] and  $Z = 4$  (Toman, 1977), whose monoclinic structure deviates only slightly from the approximate orthorhombic structure determined previously (Heritsch, 1938). Interestingly, the silicate mineral andalusite,  $\text{Al}_2\text{SiO}_5$ ,  $Pnmm$ ,  $Z = 4$  (Burnham and Buerger, 1961) is isostructural with the last series of arsenates and phosphates, as was pointed out by Strunz (1936).

The synthetic compounds  $\text{Cd}_2\text{PO}_4\text{F}$  and  $\text{Cu}_2\text{PO}_4\text{F}$  with space group  $C2/c$  (equivalent to  $I2/a$ ) are isostructural with triplite (Rea and Kostiner, 1974; 1976).  $\text{Co}_2\text{AsO}_4\text{OH}$  is isostructural with adamite (Riffel *et al.*, 1975), whereas  $\text{Sn}_2\text{PO}_4\text{OH}$  with space group  $P2_1/n$  and  $Z = 4$  has a distinct structure unrelated to the others (Jordan *et al.*, 1976). Several analogous compounds with chlorine instead of F/OH display still other structural types, as could be expected from the larger size of the  $\text{Cl}^-$  ion. Another related group of minerals has the general formula  $\text{AB}(\text{XO}_4)_2$ , where A and B may be two divalent metal atoms of different size (Be, Mn, Mg, Fe, Zn, Cu, Ba, Pb) or one monovalent and one trivalent metal atom (Li, Na; Al, Fe). Included in this group are also some vanadates. A number of distinct structure types are known among these compounds.

The crystal structure of althausite is unique among the structures of these minerals and synthetic compounds. Wagnerite,  $\text{Mg}_2\text{PO}_4\text{F}$ , which is chemically close to althausite, also has Mg in both 5- and 6-coordination, but has a much more complicated structure, and its eight structurally distinct Mg polyhedra are connected differently. Another mineral that is chemically close to althausite is holtedahlite,  $\text{Mg}_2\text{PO}_4\text{OH}$  (Raade and Mladeck, 1979), which is hexagonal and must belong to yet another structure type. A structure determination of this mineral is in progress. The iron analogue of holtedahlite is satterlyite, recently described by Mandarino *et al.* (1978).

Althausite has some formal structural features in common with the minerals libethenite-olivenite-adamite-eveite-andalusite, in that they contain similar cation polyhedra with 5- and 6-coordination and the same kind of edge-sharing octahedral chains. The althausite structure, with a cell volume about twice that of the others, has two different  $\text{Mg}^{\text{V}}$  and OH/F sites, so that other aspects of the structures show no close relationship.

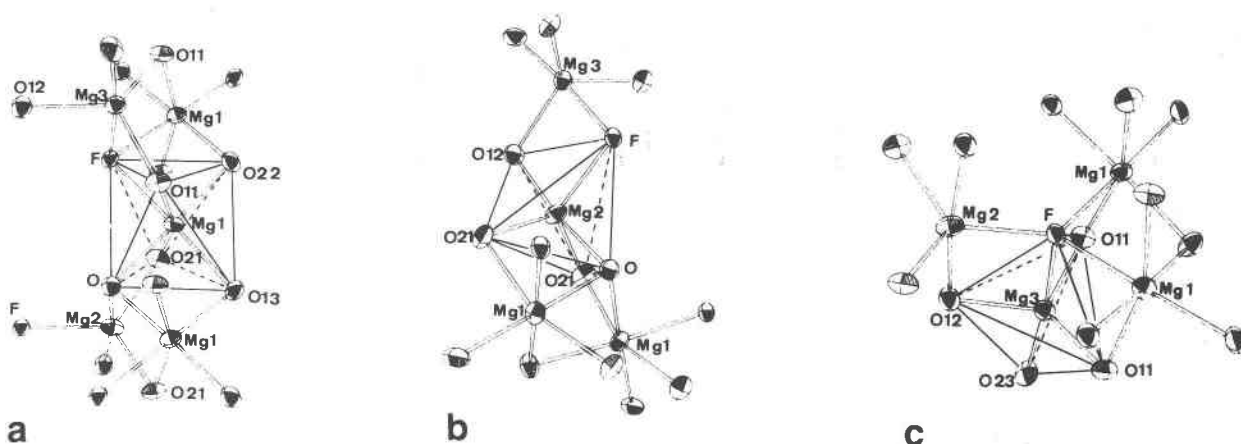


Fig. 3. The three different Mg coordination polyhedra in althausite with their nearest surroundings; ORTEP drawings, showing ellipsoids of thermal vibration. (a) The  $[\text{Mg}(1)\text{O}_4(\text{OH})\text{F}]$  distorted octahedra form chains parallel to  $b$  by edge-sharing, and are in turn connected with  $\text{Mg}^{\text{V}}(2)$  and  $\text{Mg}^{\text{V}}(3)$  polyhedra, also through edge-sharing. (b) The  $[\text{Mg}(2)\text{O}_3(\text{OH})\text{F}]$  distorted trigonal bipyramid shares edges with two  $\text{Mg}^{\text{VI}}(1)$  polyhedra and one  $\text{Mg}^{\text{V}}(3)$  polyhedron. (c) The  $[\text{Mg}(3)\text{O}_4\text{F}]$  distorted trigonal bipyramid shares edges with two  $\text{Mg}^{\text{VI}}(1)$  polyhedra and one  $\text{Mg}^{\text{V}}(2)$  polyhedron.

### Cleavage

The perfect pinacoidal cleavage along  $\{001\}$  and the distinct prismatic cleavage along  $\{101\}$  in althausite are plausibly explained on the basis of structural information. These cleavages occur along planes which cross relatively few bonds and are formed by breaking bonds between phosphate groups and Mg polyhedra (Figs. 1 and 2). The chains of  $[\text{MgO}_4(\text{OH})\text{F}]$  octahedra running parallel to the  $b$  axis, and which apparently constitute a strong entity in the structure, are left intact.

Note that the two cleavages in andalusite, distinct along  $\{110\}$  and indistinct along  $\{100\}$ , are comparable to the cleavages in althausite, and leave the  $\text{AlO}_6$  chains which run parallel to the  $c$  axis unbro-

ken (based on the setting  $c < a < b$ , space group  $Pn\bar{m}$ ). However, for the isostructural minerals libethenite, olivenite, adamite, and eveite, quite different cleavage directions are quoted in the literature, namely indistinct  $\{100\}$  and  $\{010\}$  for libethenite, indistinct  $\{011\}$  and  $\{110\}$  for olivenite, good  $\{101\}$  and poor  $\{010\}$  for adamite, and fair  $\{101\}$  for eveite, all cleavages apparently given for the same setting  $c < a < b$  (cf. e.g. Roberts *et al.*, 1974). It should be expected that the cleavages of a series of isostructural minerals were comparable, of course not in quality, but at least in direction. Cleavages reported for olivenite, adamite, and eveite, involving a breaking of the octahedral chains running parallel to the  $c$  axes, must therefore be regarded as questionable.

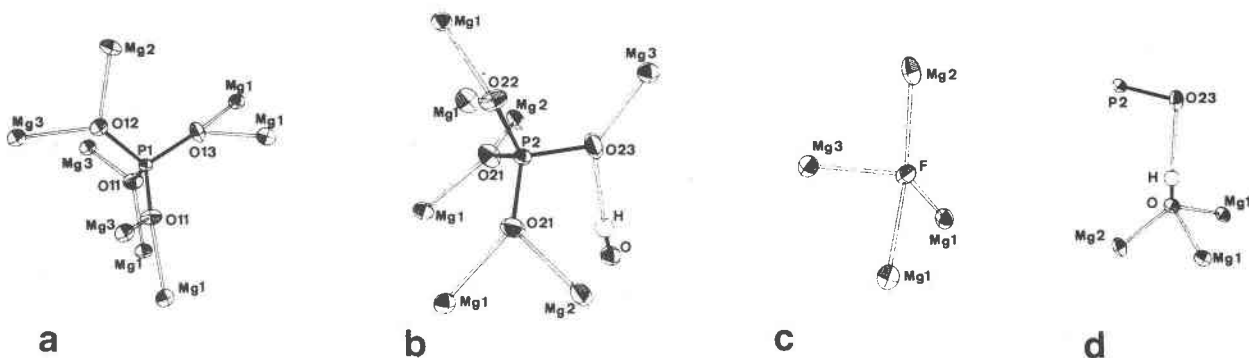


Fig. 4. ORTEP drawings, showing ellipsoids of thermal vibration. (a and b) The two non-equivalent  $\text{PO}_4$  tetrahedra in althausite and the connections between their oxygen atoms and the neighboring Mg atoms. (c) The bonding arrangement of the F atom. In synthetic althausite this site may also be occupied by hydroxyl, with the O-H pointing in the opposite direction to the O-Mg(3) bond. (d) The bonding arrangements around the OH site.

Table 4. Bond-strength calculation for althausite (valence units)

	Mg(1)	Mg(2)	Mg(3)	P(1)	P(2)	H	$\Sigma$
O(11)	0.330		0.379 x 2+	1.249 x 2+			1.958 x 2+
O(12)		0.410	0.409 0.042 x 2+ x 2+	1.225			2.128
O(13)	0.359 x 2+	0.063 0.045		1.232			2.058
O(21)	0.326 0.043 0.037	0.368 x 2+			1.229 x 2+		2.003 x 2+
O(22)	0.388 x 2+		0.052 0.048		1.225		2.101
O(23)		0.041 x 2+ x 2+	0.452		1.314	0.10	1.948
O	0.381 x 2+	0.397				0.90	2.059
F	0.236 x 2+	0.266	0.242				0.980
$\Sigma$	2.100 x 2+	1.999	2.045	4.955	4.997	1.00	19.196

Computed from the empirical bond-strength - bond-length relations of Brown and Wu (1976), Brown (1976) and Brown (1977).

### Bond lengths and bond angles

The mean P-O bond length (corrected for libration) is 1.548Å with a standard deviation from the mean of 0.003Å; the average is taken over seven of the P-O bonds. The P(2)-O(23) bond is significantly shorter, 1.526Å, indicating a smaller negative net charge on this oxygen atom. The reason is clearly indicated by the coordination of the phosphate oxygen atoms. O(23) is coordinated to one Mg(3) ion and is also engaged as acceptor in a hydrogen bond (Fig. 4b), whereas all the other phosphate oxygen atoms are each coordinated to two Mg ions.

The O-H bond length (0.78Å) is shorter than the accepted O-H bond, which is 0.95Å or longer if the hydrogen is engaged in hydrogen bonding. This is because the X-ray method measures the position of electron density maxima rather than the position of the atomic nuclei.

The distortion of the cation polyhedra conforms to the generally accepted rule for ionic structures, that shared edges tend to be shorter than unshared ones. This may be verified by inspection of bond angles with magnesium ions as the central atom as given in Table 3.

### Bond-strength calculations

A bond-strength table for althausite is presented in Table 4, and is based on an 'ideal' structure with fully occupied OH<sup>-</sup> and F<sup>-</sup> sites. The P-O bond lengths utilized in the calculation are those uncorrected for libration, since the empirical curves relating bond strengths and bond lengths are based on distances uncorrected for thermal motion (Brown and Shannon, 1973). As can be seen from the table, the bond-strength sums for althausite are satisfactory, with a maximum deviation of 6.4 percent for O(12). However, to achieve this it was necessary also to consider the contributions from the second-closest neighbors at distances (Mg-O) from 3.09 to 3.49Å, although the calculated bond strengths may not be very accurate for such long bonds. The large degree of distortion of the coordination polyhedra in althausite makes the necessity of such an approach quite reasonable.

We have also calculated the bond sums for wagnerite (Table 5). The sums for Mg are systematically too low, and also in this case it might be necessary to take into account the contributions from oxygen atoms farther away. Similarly, highly distorted Mg

polyhedra occur in the wagnerite structure as in the althausite structure. Note the significantly low sums around two of the  $F^-$  ions, F(2) and F(3). Wagnerites may contain substantial amounts of  $OH^-$  (see below), and possibly this hydroxyl is preferably substituted in two of the four  $F^-$  sites, so as to produce a partly ordered structure with regard to  $OH^-/F^-$ . However, further discussion of the bond-strength sums for wagnerite is better postponed until a refined structure has been determined for a wagnerite with known F:OH ratio. We hope to undertake such an investigation at a later date.

#### Distribution of $OH^-$ and $F^-$

The  $OH^-$  and  $F^-$  anions have approximately the same size and are frequently found to replace each other completely. A well-known example among the phosphates is the pair fluorapatite-hydroxyapatite. However, in some instances the OH and F analogues may have different space groups and cell dimensions and show a limited degree of solid solution, although the structures are commonly closely related. Examples, again taken from the phosphate group of minerals, are the pairs zwieselite/triplite,  $(Fe,Mn)_2PO_4F$ , and wolfeite/triploidite,  $(Fe,Mn)_2PO_4OH$ , mentioned above. The main difference between these structures is that  $F^-$  occurs completely disordered between two possible sites in triplite, whereas  $OH^-$  is ordered in triploidite, probably owing to the dipolar character of the  $OH^-$  (Waldrop, 1970). The site splitting in natural triplite may be caused by the presence of large amounts of the smaller  $Mg^{2+}$  ion, since the pure compound  $Mn_2PO_4F$  does not show this disorder (Rea and Kostiner, 1972).

Apart from the similarity in size between  $OH^-$  and  $F^-$ , these anions have otherwise very different properties with regard to polarizability and electronegativity. Replacement and ordering of  $OH^-$  and  $F^-$  in crystal structures are thus generally controlled by the coordination and kind of ligands of the structural sites. On this basis, the high degree of ordering between  $OH^-$  and  $F^-$  is readily explained in the case of althausite, where the two available sites have quite different environments and one of them is preferred by  $OH^-$ , the other by  $F^-$  (Fig. 4, c and d). In wagnerite also, some ordering of  $OH^-$  and  $F^-$  is indicated (see preceding subchapter). These anions may be, to a large extent, ordered in many other structures, but in most cases this is difficult to detect by X-ray diffraction methods. However, a  $OH^-/F^-$  anion order-

Table 5. Calculated bond-strength sums ( $p$ ) for wagnerite

Atom	$p$ (v.u.)	$\Delta^*$	Atom	$p$ (v.u.)	$\Delta^*$
$Mg^V(1)$	1.94	3.0	0(1)	2.00	0.0
$Mg^V(3)$	1.91	4.5	0(2)	1.93	3.5
$Mg^V(5)$	1.81	9.5	0(3)	1.99	0.5
$Mg^V(7)$	1.82	9.0	0(4)	1.93	3.5
$Mg^{VI}(2)$	1.97	1.5	0(5)	1.96	2.0
$Mg^{VI}(4)$	1.95	2.5	0(6)	2.00	0.0
$Mg^{VI}(6)$	1.86	7.0	0(7)	1.99	0.5
$Mg^{VI}(8)$	1.85	7.5	0(8)	1.96	2.0
P(1)	5.00	0.0	0(9)	1.97	1.5
P(2)	5.01	0.2	0(10)	1.97	1.5
P(3)	5.08	1.6	0(11)	1.99	0.5
P(4)	4.97	0.6	0(12)	2.02	1.0
F(1)	0.95	5.0	0(13)	2.06	3.0
F(2)	0.86	14.0	0(14)	1.86	7.0
F(3)	0.86	14.0	0(15)	2.01	0.5
F(4)	0.95	5.0	0(16)	1.94	3.0

Computed from the empirical bond-strength - bond-length relations of Brown and Wu (1976) and Brown (1977). Based on the structure determination of Coda *et al.* (1967).

\* Percentage difference between valence and  $p$ .

ing has been found in the apatite structure by means of neutron diffraction (Nozik, 1978).

The availability of F, the temperature and pressure of formation, and also the oxygen fugacity of the environment are factors that control the degree of replacement of  $F^-$  and  $OH^-$  in minerals. As discussed below, a completely F-free althausite has been synthesized, and this shows that F is not an essential constituent of the althausite structure.

#### The defect structure of althausite

Chemical evidence presented in the Introduction and the results of the structure determination have confirmed the original assumption made by Raade and Tysseland (1975) that althausite has a defect structure with partly empty (OH,F) sites. The structural data show that the  $OH^-$  occurs mainly in one of two distinct sites which has a full occupancy, and the  $F^-$  ions and empty positions are confined to the other site [population factor 81(1) percent]. The position of the  $O^{2-}$  ions has not been proven, but considering the empirical coefficients obtained from the chemical analysis,  $(OH_{0.37}F_{0.25}O_{0.19}\square_{0.19})$ , it is reasonable to assume that both  $OH^-$  and  $O^{2-}$  occupy the position that was found to be fully populated. The structural-

chemical formula for althausite should thus be expressed as  $Mg_4(PO_4)_2(OH,O)(F,\square)$ , with possibly some OH in the F site.

The occurrence of  $OH^-$  and  $F^-$  in 'double channels' along  $b$  may be a clue to the existence and formation of a defect althausite structure, in that these channels may allow water to escape from the mineral (perhaps caused by a strong thermal event which may have affected these polymetamorphic serpentine–magnesite deposits), and further that the channels may provide a possibility for adjustments of atomic positions to compensate for the electrostatic imbalances brought about by the  $O^{2-}$  ions and empty positions. An analogy of great importance is provided by the apatite structure, which also contains 'channels' (along  $c$ ) filled with  $OH^-/F^-/Cl^-$  and which has also been described with partially as well as completely empty halide sites (e.g. McConnell, 1973 for a review).

#### Synthetic work

Some preliminary results of hydrothermal syntheses performed by G. Raade at Mineralogisches Institut der Universität Karlsruhe are presented here, since they have some bearing on the discussion of the althausite structure.

At present, results from runs made at the following pressures and temperatures are available: 1 kbar (650°C), 2 kbar (550, 650°C), 4 kbar (400, 500, 550, 600, 650°C), and 7 kbar (600°C). From mixtures of  $MgHPO_4 \cdot 3H_2O$ ,  $MgF_2$ , and  $Mg(OH)_2$  with the ratio  $Mg:P:F = 2:1:1$ , only wagnerite has been obtained as a pure phase with just a trace of OH as shown by infrared spectroscopy. From a similar mixture with  $OH:F = 1:1$ , a pure wagnerite phase is obtained in some cases, and mixtures of wagnerite and varying amounts of althausite in others. The formation of althausite is clearly favored by higher temperatures/lower pressures compared to wagnerite, which is consistent with the denser packing of the wagnerite structure (Table 3 in Raade and Mladeck, 1979). This wagnerite contains considerable amounts of OH and has a somewhat larger cell volume than the nearly pure F-wagnerite. Also the althausite is a OH/F-bearing variety.

More interesting in the present context are the runs made with F-free reactants, *i.e.* with  $Mg:P:OH = 2:1:1$ . In these cases mixtures of varying amounts of OH-althausite and holtedahlite are produced, together with several unknown phases. This althausite has a somewhat larger cell volume than the OH/F variety.

Further experiments to elucidate the phase relationships in the system  $Mg_2PO_4F$ – $Mg_2PO_4OH$  are being undertaken. The preliminary results indicate that there exist two series: from F-wagnerite to OH/F-wagnerite, and from OH-althausite to OH/F-althausite, but the limits of the substitutions have not yet been determined. Holtedahlite has only been obtained as a F-free phase.

The partially ordered site distributions of  $OH^-$  and  $F^-$  in natural althausite and possibly also in wagnerite were discussed above. In synthetic OH-althausite, the  $OH^-$  ions must occur in two different structural positions. This is clearly corroborated by the infrared spectroscopic study.

#### Infrared spectroscopy

The O–H stretching frequency of natural althausite occurs at  $3510\text{ cm}^{-1}$  (Raade and Tysseland, 1975). Using the Lippincott–Schroeder curve for the theoretical relation between O–H frequency shift and hydrogen bond length (Lippincott and Schroeder, 1955), this gives an O–H ... O distance of *ca.*  $2.94\text{ \AA}$  in althausite, in good agreement with the value  $2.939(2)\text{ \AA}$  obtained from the structure determination.

Synthetic OH-althausite formed at 4 kbar and  $600^\circ\text{C}$  shows a distinct splitting of the O–H stretching band, with sharp peaks at  $3510$  and  $3530\text{ cm}^{-1}$ . The latter frequency corresponds to a slightly larger O–H ... O distance of *ca.*  $2.97\text{ \AA}$  according to the Lippincott–Schroeder relation. This must imply an adjustment of distances compared to the structure of natural althausite, where F–O(21) is  $2.87\text{ \AA}$  and F–O(H) is  $2.94\text{ \AA}$ . If  $OH^-$  were substituted for  $F^-$  in the althausite structure with the oxygen occupying exactly the same position as fluorine, a bifurcated hydrogen bonding to the two nearest oxygens O(21) and O(H) would be the most likely result (Fig. 3c). This means that the O atom is both a donor and an acceptor of a hydrogen bond. However, an adjustment of distances could result in one of the bifurcated bonds being preferred. As an ultimate corollary of these changes, it is even possible that the space group could be different for the OH-althausite, *e.g.* if the symmetry center is lost.

Natural wagnerite is often assumed to represent the pure F end-member, and  $H_2O$  is rarely reported in the analyses. However, wagnerite from Bamble shows important amounts of OH, according to the infrared spectrum (*cf.* Raade and Tysseland, 1975), and wagnerite from Sweden has a ratio  $F:OH = 1:0.81$  (Henriques, 1956). The substitution of  $OH^-$  for  $F^-$  has a substantial influence on the refractive in-

dices, which are increased, and this is why the points for the Swedish wagnerite fall off the lines on the diagram presented by Propach (1976) to relate values of refractive indices and Fe, Mn contents for wagnerites. The O–H stretching frequency for natural as well as synthetic wagnerites occurs at 3570–3580  $\text{cm}^{-1}$ , indicating an O–H ... O bond distance of ca. 3.03 Å, which is similar to that of holtedahlite (Raade and Mladeck, 1979).

### Acknowledgments

The synthetic work from which some preliminary results are presented here was made possible through a fellowship to G. Raade from the Alexander von Humboldt-Stiftung. The infrared spectra were recorded at Institut für Kristallographie, Universität Karlsruhe. We thank W. Smykatz-Kloss of Mineralogisches Institut, Universität Karlsruhe for the TGA runs and C. J. Elliott at Department of Mineralogy, British Museum (Natural History) for the  $\text{H}_2\text{O}$  and  $\text{CO}_2$  determinations. W. L. Griffin at Mineralogisk-Geologisk Museum, University of Oslo gave assistance with the microprobe analyses. A crystal of althausite was put at our disposal for measurement by R. Hansen. We thank Professors E. Althaus and H. Wondratschek for their comments on the manuscript.

### References

- Brown, I. D. (1976) On the geometry of O–H...O hydrogen bonds. *Acta Crystallogr.*, *A32*, 24–31.
- (1977) Predicting bond lengths in inorganic crystals. *Acta Crystallogr.*, *B33*, 1305–1310.
- and R. D. Shannon (1973) Empirical bond-strength–bond-length curves for oxides. *Acta Crystallogr.*, *A29*, 266–282.
- and K. K. Wu (1976) Empirical parameters for calculating cation–oxygen bond valences. *Acta Crystallogr.*, *B32*, 1957–1959.
- Burnham, C. W. and M. J. Buerger (1961) Refinement of the crystal structure of andalusite. *Z. Kristallogr.*, *115*, 269–290.
- Cocco, G., L. Fanfani and P. F. Zanazzi (1966) The crystal structure of tarbutite,  $\text{Zn}_2(\text{OH})\text{PO}_4$ . *Z. Kristallogr.*, *123*, 321–329.
- Coda, A., G. Giuseppetti and C. Tadini (1967) The crystal structure of wagnerite. *Rend. Accad. Naz. Lincei*, *43*, 212–224.
- Dal Negro, A., G. Giuseppetti and J. M. Martin Pozas (1974) The crystal structure of sarkinite,  $\text{Mn}_2\text{AsO}_4(\text{OH})$ . *Tschermaks Mineral. Petrogr. Mitt.*, *21*, 246–260.
- Doyle, P. A. and P. S. Turner (1968) Relativistic Hartree–Fock X-ray and electron scattering factors. *Acta Crystallogr.*, *A24*, 390–397.
- Germain, G., P. Main and M. M. Woolfson (1971) The application of phase relationships to complex structures. III. The optimum use of phase relationships. *Acta Crystallogr.*, *A27*, 368–376.
- Groth, P. (1973) Crystallographic computer programs for CYBER-74. *Acta Chem. Scand.*, *27*, 1837.
- Hawthorne, F. C. (1976) A refinement of the crystal structure of adamite. *Can. Mineral.*, *14*, 143–148.
- Henriques, Å. (1956) An iron-rich wagnerite, formerly named talktriplite, from Hällsjöberget (Horrsjöberget), Sweden. *Ark. Mineral. Geol.*, *2*, 149–153.
- Heritsch, H. (1938) Die Struktur des Olivenites  $\text{Cu}_2(\text{OH})(\text{AsO}_4)$ . *Z. Kristallogr.*, *99*, 466–479.
- Hill, R. J. (1976) The crystal structure and infrared properties of adamite. *Am. Mineral.*, *61*, 979–986.
- Jordan, T. H., L. W. Schroeder, B. Dickens and W. E. Brown (1976) Crystal structure of stannous hydroxide phosphate, a reaction product of stannous fluoride and apatite. *Inorg. Chem.*, *15*, 1810–1814.
- Lippincott, E. R. and R. Schroeder (1955) One-dimensional model of the hydrogen bond. *J. Chem. Phys.*, *23*, 1099–1106.
- Mandarino, J. A., B. D. Sturman and M. I. Corlett (1978) Satterlyite, a new hydroxyl-bearing ferrous phosphate from the Big Fish River area, Yukon Territory. *Can. Mineral.*, *16*, 411–413.
- McConnell, D. (1973) *Apatite*. Springer-Verlag, New York.
- Moore, P. B. and J. R. Smyth (1968) Crystal chemistry of the basic manganese arsenates: III. The crystal structure of eveite,  $\text{Mn}_2(\text{OH})(\text{AsO}_4)$ . *Am. Mineral.*, *53*, 1841–1845.
- Nozik, Yu. Z. (1978) Neutron diffraction methods for investigation in the structure of minerals (abstr.). *Phys. Chem. Minerals*, *3*, 83–84.
- Propach, G. (1976) Brechungsindizes und Dichten zum Bestimmen von Wagneriten  $(\text{Mg,Fe})_2\text{PO}_4\text{F}$ . *Neues Jahrb. Mineral. Monatsh.*, 159–161.
- Raade, G. and M. H. Mladeck (1979) Holtedahlite, a new magnesium phosphate from Modum, Norway. *Lithos*, *12*, 283–287.
- and M. Tysseland (1975) Althausite, a new mineral from Modum, Norway. *Lithos*, *8*, 215–219.
- Rea, J. R. and E. Kostiner (1972) The crystal structure of manganese fluorophosphate,  $\text{Mn}_2(\text{PO}_4)\text{F}$ . *Acta Crystallogr.*, *B28*, 2525–2529.
- and ——— (1974) Cadmium fluorophosphate,  $\text{Cd}_2(\text{PO}_4)\text{F}$ . *Acta Crystallogr.*, *B30*, 2901–2903.
- and ——— (1976) The crystal structure of copper fluorophosphate,  $\text{Cu}_2(\text{PO}_4)\text{F}$ . *Acta Crystallogr.*, *B32*, 1944–1947.
- Richmond, W. E. (1940) Crystal chemistry of the phosphates, arsenates and vanadates of the type  $\text{A}_2\text{XO}_4(\text{Z})$ . *Am. Mineral.*, *25*, 441–479.
- Riffel, H., F. Zettler and H. Hess (1975) Die Kristallstruktur von  $\text{Co}_2(\text{OH})\text{AsO}_4$ . *Neues Jahrb. Mineral. Monatsh.*, 514–517.
- Roberts, W. L., G. R. Rapp, Jr. and J. Weber (1974) *Encyclopedia of Minerals*. Van Nostrand Reinhold, New York.
- Stewart, R. F., E. R. Davidson and W. T. Simpson (1965) Coherent X-ray scattering for the hydrogen atom in the hydrogen molecule. *J. Chem. Phys.*, *42*, 3175–3187.
- Strunz, H. (1936) Vergleichende röntgenographische und morphologische Untersuchung von Andalusit  $(\text{AlO})\text{AlSiO}_6$ , Libethenit  $(\text{CuOH})\text{CuPO}_4$  und Adamin  $(\text{ZnOH})\text{ZnAsO}_4$ . *Z. Kristallogr.*, *94*, 60–73.
- Terpstra, P. and L. W. Codd (1961) *Crystallography*. Longmans, London.
- Toman, K. (1977) The symmetry and crystal structure of olivenite. *Acta Crystallogr.*, *B33*, 2628–2631.
- Waldrop, L. (1969) The crystal structure of triplite,  $(\text{Mn,Fe})_2\text{FPO}_4$ . *Z. Kristallogr.*, *130*, 1–14.
- (1970) The crystal structure of triploidite and its relation to the structures of other minerals of the triplite–triploidite group. *Z. Kristallogr.*, *131*, 1–20.
- Walitzki, E. M. (1963) Strukturverfeinerung von Libethenit  $\text{Cu}_2(\text{OH})\text{PO}_4$ . *Tschermaks Mineral. Petrogr. Mitt.*, *8*, 614–624.